A tunable phononic crystal system for elastic ultrasonic wave control

View Online   Export Citation   CrossMark

Yihao Song[1] and Yanfeng Shen[1,2,a)]

AFFILIATIONS

[1]University of Michigan-Shanghai Jiao Tong University Joint Institute, Shanghai Jiao Tong University, Shanghai 200240, China
[2]Shanghai Key Laboratory for Digital Maintenance of Buildings and Infrastructure, Shanghai 200240, China

[a)]Author to whom correspondence should be addressed: yanfeng.shen@sjtu.edu.cn

ABSTRACT

Tunable phononic crystals (PCs) are burgeoning within the engineering communities due to their adjustable capabilities for manipulating elastic waves. In this Letter, a shape memory alloy (SMA) stubbed PC is elaborated to achieve the tunable bandgaps for the control of ultrasonic waves. The tunable mechanism stems from the phase transformation of the SMA between the martensite at low temperature and the austenite at high temperature. Both numerical modeling and experimental verification are conducted to validate the achievement of the controllable stop band properties. The proposed SMA PC design could be broadened to numerous promising applications, e.g., ultrasonic wave waveguiding, flat-lens focusing, and mechanical frequency filtering, possessing enabling potential for highly adjustable wave manipulation.

Local resonant based phononic crystals (PCs) have been widely investigated over the past decades due to their superb capabilities for vibration and elastic wave control. In particular, with the designed microstructures, the bizarre phenomena can be achieved, e.g., negative mass density[1–4] and negative bulk modulus,[5–8] rendering numerous promising applications. Unfortunately, most PCs are featured by a passive response, once the unit cells were fabricated, considerably limiting their adaptiveness for varying demands. On the other hand, tunable PCs are drawing increasing attention for their adjustable and adaptive features. In this sense, one natural logic incorporates active materials into the design of the unit cells. Pioneer research efforts have been devoted to realize the controllable and programmable wave manipulation using the electrorheological elastomer and piezoelectric-patch PCs.[9,10] Shape memory alloy (SMA) is another special energy transduction material, exhibiting unique thermal and mechanical behaviors. The mechanism behind the unique properties resides in the phase transformation between the martensite at low temperature and the austenite at high temperature. The peculiar elastic modulus variation originated from the crystallographic structure evolution would facilitate a controllable microstructure design. To date, pioneer investigations have been carried out for adopting SMAs for vibration absorbers and tunable PCs in low frequency regime.[11–20] However, few investigations have been performed toward controlling the multimodal ultrasonic guided waves via the SMA structures with experimental validations. This study strives to utilize the specific stiffness-change-property due to the phase transformation phenomenon of the SMAs under a thermal load for designing a bandgap-adjustable PC. The marvelous wave manipulation capability of the tunable PCs may possess great application potential in Nondestructive Evaluation (NDE) and Structural Health Monitoring (SHM), such as adaptively filtering out the inherent nonlinearity in the nonlinear ultrasonic techniques or focusing the Lamb waves to arbitrary directions where the receiver performance can be strengthened with the amplified energy,[21,22] enhancing the accuracy of damage identification and quantification.

Figure 1(a) illustrates the schematic diagram of the proposed unit cell. It is comprised of an SMA cylinder directly bonded to a 2 mm thickness aluminum substrate plate. The height and the radius of the cylinder are 9 and 1.75 mm, respectively. It should be noted that the design parameters would significantly influence the performance of the PC system. The finite element model (FEM) of the unit cell presented in Fig. 1(b) was constructed using the commercial software package ANSYS 15.0. The material properties used for the unit cells are the following: Young's modulus $E_{Al} = 70$ Gpa; Poisson's ratio $\vartheta_{Al} = 0.33$; $\vartheta_{SMA} = 0.33$; density $\rho_{Al} = 2700 \text{ kg/m}^3$; $\rho_{SMA} = 6400 \text{ kg/m}^3$. The phase transformation between martensitic state and austenitic state of the SMAs due to the temperature variation was numerically simulated by changing the elastic moduli of the stub. Theoretically, the elastic modulus of SMA would present a quasi-linear relationship with temperature in the phase transition zone. It is rational to deduce that the wave propagation characteristics inside the PC systems would also exhibit a quasi-linear variation performance as
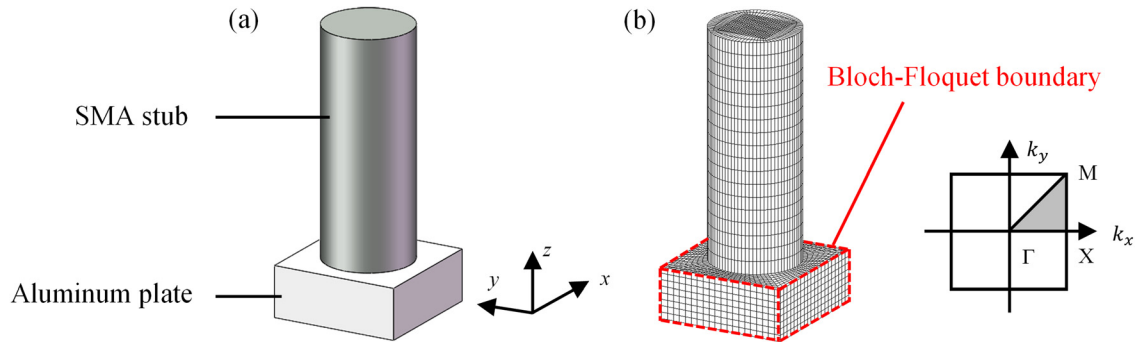
FIG. 1. (a) Schematic diagram of the unit cell. (b) Finite element model and the irreducible first Brillouin zone with primitive vectors.

the temperature gradually increases from both conceptual and numerical point of view. However, in practice, the transition zone is quite narrow and hard to capture. Thus, in this study, the research effort is focused on demonstrating the tunable feature of wave propagation control. As a consequence, only the PC structures in the fully martensitic and austenitic state were considered. The transition behavior of the proposed system may be presented in a future study with enriched details and precise temperature control apparatus. Martensitic stiffness was set to be 30 MPa, while that of the austenite was assumed to be 70 MPa[15] (the estimated values were denoted by SuZhou Chuan Mao Materials Co., Ltd., the manufacturer of the SMAs in the experimental validation section). Modal analysis was performed by treating the unit cell with Bloch–Floquet boundary condition for deriving the ideal frequency-wavenumber domain dispersion characteristics of the elastic waves propagating through an infinite PC plate.

The calculated band structures of unit cells in different material phase states are displayed in Fig. 2. Figure 2(c) corresponds to the band structure of the unit cell in the martensite phase state shown in Fig. 2(a), whereas Fig. 2(d) denotes the dispersion relation of the unit cell presented in austenitic phase depicted by Fig. 2(b). It can be observed that the complete stopbands were developed in both cases, indicating that the ultrasonic guided waves cannot pass through the PC system within the corresponding frequency region. The martensite state structure with a lower elastic modulus developed a bandgap appearing from 54.12 to 66.51 kHz. On the other hand, the bandgap shifted upwards to a higher frequency range from 75.92 to 97.41 kHz, when the SMA state transformed to the austenite which possesses a larger elastic modulus. Such a result depicts a remarkable bandgap location movement, demonstrating the tunable property of the bandgap in the proposed SMA pillared PC. This phenomenon demonstrates the feasibility to adaptively control the ultrasonic waves through
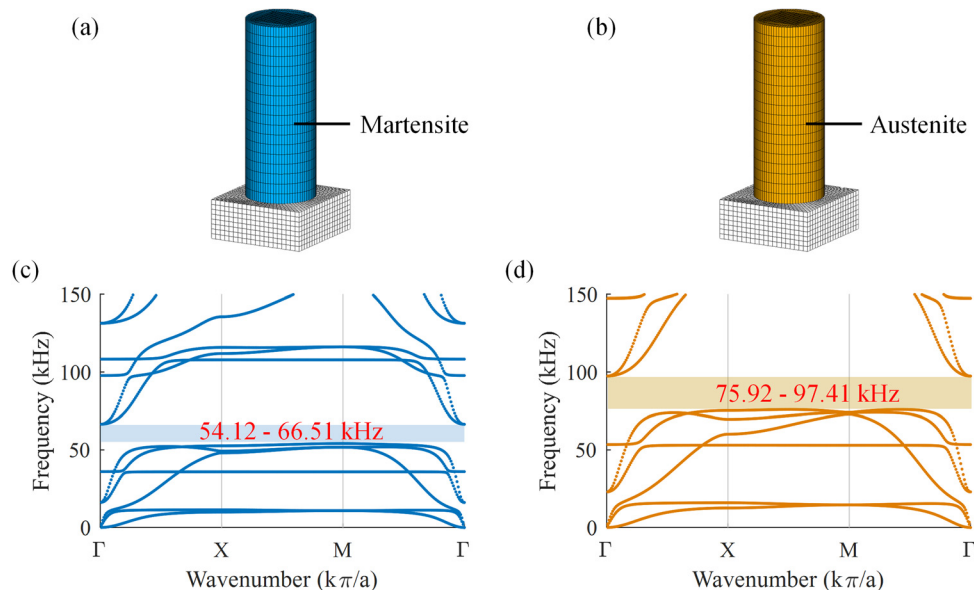

FIG. 2. (a) Finite element model of the unit cell in the martensite phase state. (b) Finite element model of the unit cell in the austenite phase state. (c) Band structure of the unit cell in the martensite phase state. (d) Band structure of the unit cell in austenite phase state.

the SMA substructure designs by adjusting the thermal loads on the phase changing element.

To further demonstrate the elastic wave attenuation capability and investigate the adjustable bandgap property of the proposed tunable PC, harmonic analysis was performed to attain the spectral response of an aluminum beam bonded with ten unit cells. It should be noted that pioneer investigations on frequency spectra of the Lamb modes showed a negligible difference for the PC structures with either free boundary condition or periodic boundary condition.[2,23] As a consequence, in order to reduce the computational burden of the simulation and the complexity of experimental investigation, a PC stripe was simply constructed to represent the scenario of unidirectional wave propagation. Figure 3(a) illustrates the numerical model setup of the unit cell chain system. The PZT transmitter served as the wave source, generating guided waves into the stripe structure; simultaneously, the PZT receiver recorded the harmonic response, picking up the elastic waves passing through the PC system. Non-reflective boundaries were implemented on both ends of the aluminum stripe to eliminate boundary reflections.[24] It should be emphasized that a pristine pitch-catch aluminum beam with the same configuration but the absence of the PCs was also simulated as a comparative case.

To eliminate the tuning effect of the PZT sensors,[25] the frequency spectra displayed in Fig. 3(c) were obtained by taking the ratio of the

responses caught by the PZT receivers in the PC beam and that in the pristine case. Two obvious stop bands can be developed and distinguished for both martensitic and austenitic scenarios, respectively, ranging from 52.50 to 64.25 kHz and 75.50 to 96.00 kHz. Figures 3(b) and 3(c) display the comparison between the frequency spectra and the dispersion characteristics. An excellent agreement can be noticed with slight mismatches for both the martensitic and the austenitic state. The slight deviations originate from the limited number of the unit cells arranged along the x-direction in the harmonic analysis. In Fig. 4, two representative frequencies (56 and 78 kHz) were selected to demonstrate the tunable bandgap behavior of the SMA PC systems during a phase transition procedure. The equivalent stress images feature the status of the elastic wave propagation inside the PC strips. At room temperature, the SMA pillars stayed with a martensitic crystallographic structure [Fig. 4(a)]. 56 kHz fell within the bandgap which appeared at a relatively low frequency range. As a consequence, the wave energy could only pass through the first few unit cells and was stopped later on [Fig. 4(c)]. On the contrary, 78 kHz was outside the bandgap. The elastic wave penetrated the PC area with very little attenuation [Fig. 4(e)]. On the other hand, with a thermal load, the phase of SMA cylinders transformed to austenite. The stop band region moved toward the higher frequency range. In this case, the ultrasonic wave propagation was quenched at 78 kHz [Fig. 4(f)], whereas the 56 Hz
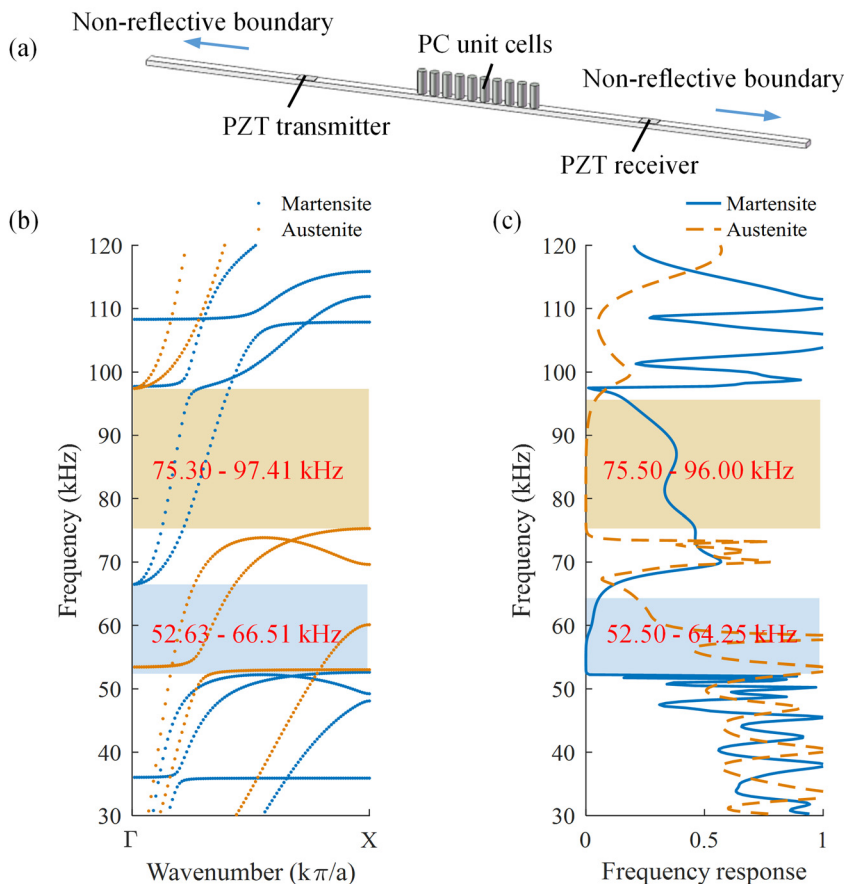

FIG. 3. (a) The numerical model setup of the PC beam in harmonic analysis. (b) The overlapped band structure of the unit cell obtained in both martensitic and austenite state from modal analysis. (c) The overlapped frequency spectrum of the PC beam in both martensitic and austenite state from harmonic analysis.
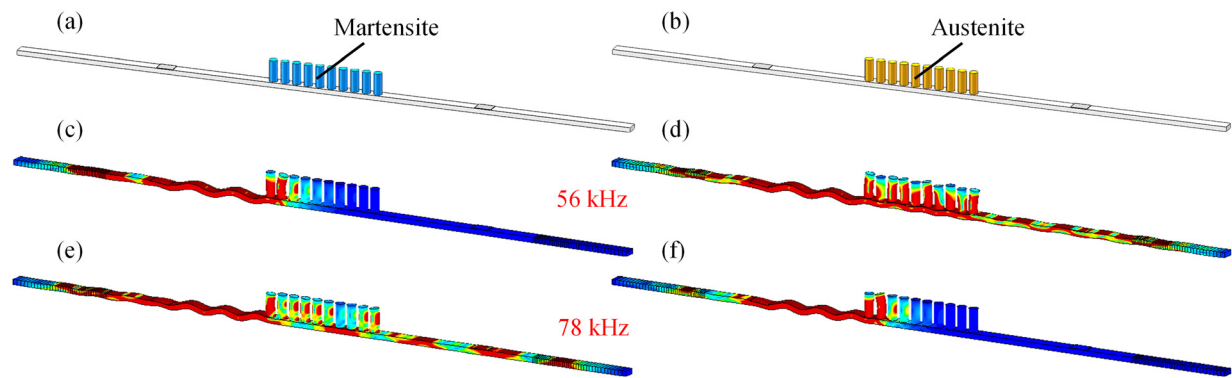
FIG. 4. The PC beam bonded with 1×10 unit cells in (a) the martensitic state and (b) the austenitic state. The equivalent stress of the PC beam in the martensitic state at (c) 56 and (e) 78 kHz. The equivalent stress of the PC beam in the austenitic state at (d) 56 and (f) 78 kHz.

became a passing frequency [Fig. 4(d)]. The frequency spectra and the equivalent stress nephograms substantiated again the marvelous adjustable property of band structures for the proposed tunable PC.

In order to validate the numerical results and verify the tunable stop band performance of the SMA PC system, experimental investigations and demonstrations with the same configurations as presented in harmonic analysis were conducted. Figure 5 illuminates the experimental setup as well as the detail features of the PC beam. The heating patch was attached on the opposite side of the stripe surface with respect to the SMA substructures, working as the thermal source [presented in Figs. 5(b) and 6(c)]. Damping clay was implemented at two far ends of the aluminum beam serving as the non-reflective boundaries. The SMA was tailored with the transformation temperature of $55\,^\circ$C (manufactured by SuZhou Chuan Mao Materials Co., Ltd.), which indicates that the SMA would sufficiently transform into austenitic phase from martensitic structure above this temperature,

considering no external mechanical loads were exerted on the pillars. A 50-count Hanning window modulated sine tone burst was first generated by the arbitrary function generator. The excitation signal was further amplified to 100 vpp by the power amplifier and applied on the PZT transmitter. Elastic ultrasonic waves generated by the PZT transmitter would propagate through the PC surface and undergo substructural interactions. Finally, the PZT receiver picked up the elastic waves arriving at the sensing location by converting the mechanical disturbances into electrical voltage collected and presented in the oscilloscope.

Two rounds of tests were carried out to demonstrate the tunable feature of the system for elastic wave control. In the first round, the PC beam worked at room temperature. In the second round, the SMA PC system would work at an elevated temperature by providing power to the heating patch. A temperature evaluation system as illuminated in Fig. 6(a) was set up for determining an adequate power inputting into
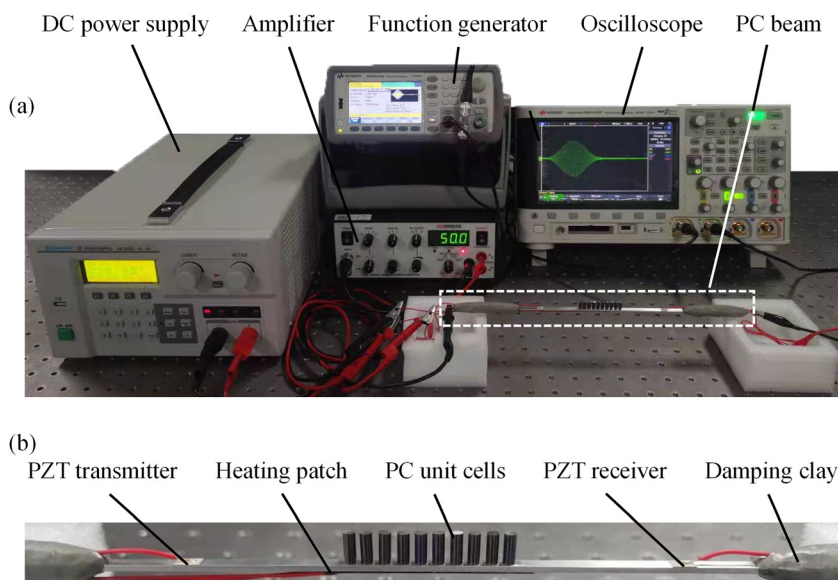

FIG. 5. (a) Experimental setup for testing the frequency spectra of the PC beam. (b) Zoom-in detail of the PC beam.
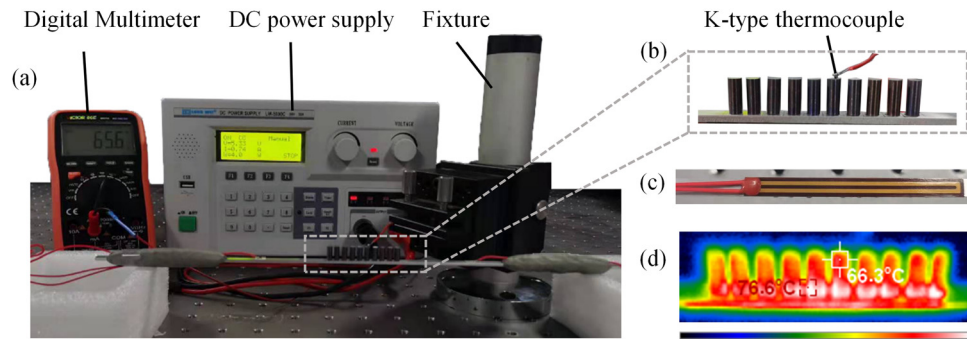
FIG. 6. (a) Temperature measurement system for the PC unit cells. (b) K-type thermocouple attached on the top surface of the SMA cylinder. (c) Front view of the heating patch. (d) Infrared image of the PC unit cell chain when the heating patch was working.

the heating patch to heat the PCs up to the transition temperature. A K-type thermocouple connected to the digital multimeter was grasped by the fixture, ensuring a tight attachment to the surface of the SMA cylinder to accurately monitor the working temperature [Fig. 6(b)]. The temperature contour plot captured by the infrared thermometry was utilized to ensure the thermal consistency [Fig. 6(d)]. A 5 W electric current input from the DC power supply proved to produce a sufficient heating capability to hold the SMA stubs above 55 °C. It should be noted that experimental tests for the pristine case (pure beam) were also conducted to eliminate the tuning effect of the PZT transducers. Figure 7 illustrates the temporal traces of the experimental sensing signals captured by PZT receiver at 56 and 78 kHz for both the room-temperature and heating-state cases. The waveforms underwent a contrary scenario for increasing frequencies when applying a thermal load, providing a more convincing evidence to demonstrate the bandgap upward-shifting phenomenon. Figure 8 demonstrates the comparison between the frequency responses derived from numerical harmonic analysis and the experimental test. The experimental frequency spectra were expressed as the ratio between the PC beam response and the pristine case through the frequency sweeping method. It should be noted that the frequency spectra from experimental measurements would not match exactly with the numerical analysis due to the small deviations on material properties, influence from the bonding layers, and the thermoelastic behaviors.
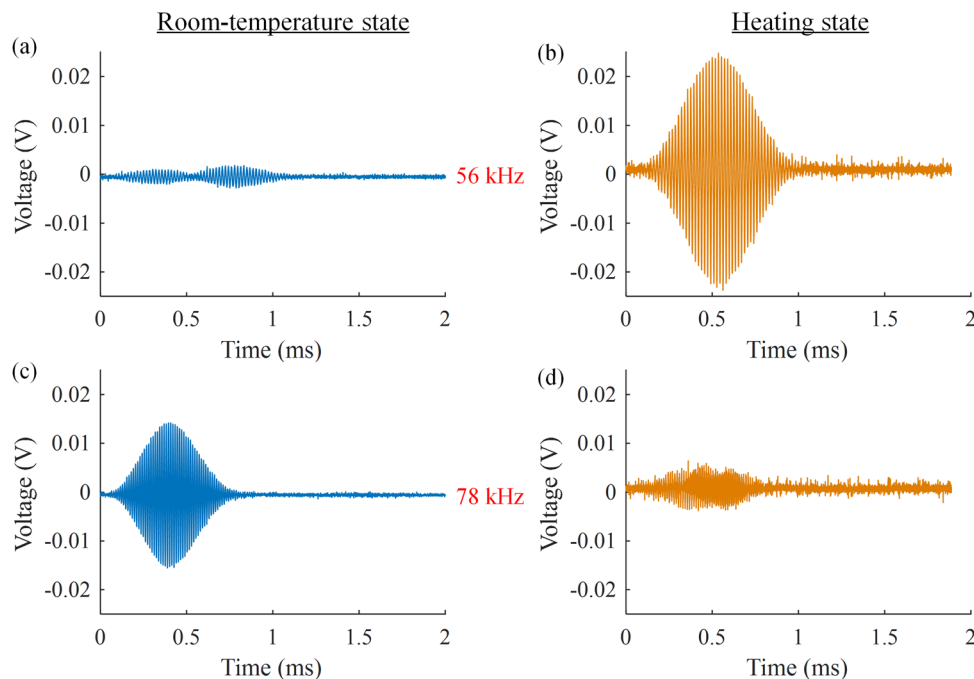

FIG. 7. Time traces of the experimental sensing signals captured by the PZT receiver for (a) 56 kHz in room-temperature state. (b) 56 kHz in heating state. (c) 78 kHz in room-temperature state. (d) 78 kHz in heating state.
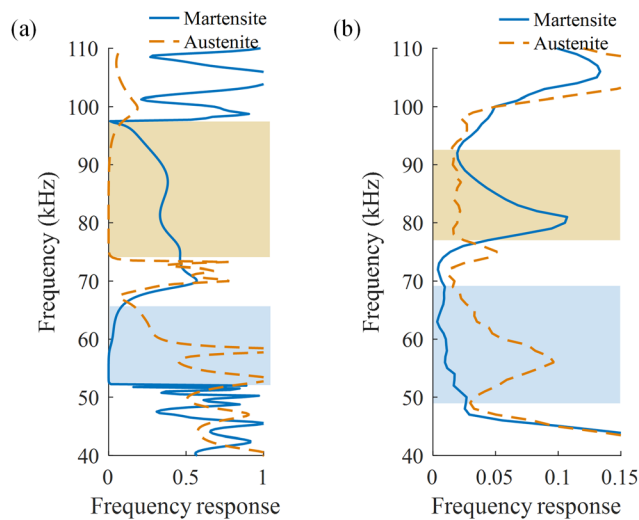
118, 224104-5

FIG. 8. (a) The overlapped frequency spectrum of the PC beam in both martensitic and austenite state from numerical harmonic analysis. (b) The overlapped frequency spectrum of the PC beam in both martensitic and austenite state from experimental test.

Nevertheless, the bandgap effect and the stop band shifting frequency region of the SMA PC system can be successfully caught, further substantiating the marvelous bandgap adjusting capability of the proposed tunable PC design. The presented investigations may pave the way for adaptive manipulation of the ultrasonic elastic waves.

In conclusion, an SMA based tunable PC with a wide adjustable ultrasonic bandgap was proposed. The underlying mechanism arises from the peculiar elastic modulus change of the SMA induced by the phase transformation under a thermal load. To demonstrate the performance of the proposed tunable PC system, the investigation was initiated via numerical simulations to explore the band structure shifting phenomenon by adopting the corresponding stiffness for martensitic and austenitic crystallographic material states. Subsequently, the frequency spectra of the unit cell chain model in the two states were derived, which verified the effectiveness of the ultrasonic stop band formation and tuning concept. It was shown that the spectra curves exhibited an excellent match with the modal analysis results. The suppression of elastic wave propagation in the PC chain revealed from the equivalent stresses plot further substantiated the ultrasonic bandgap movement features. In the end, the frequency sweeping experiments demonstrated the achievement of the stop band shift for the SMA PC from room temperature to the heating state, clearly validating the target phenomena. By tailoring the size of the PC unit cells and the phase transformation temperature of SMA, the outstanding ultrasonic elastic wave manipulation capabilities can be broadened to numerous promising applications, e.g., selective-tunnel wave waveguiding, adjustable flat-lens focusing, and adaptive mechanical frequency filtering, possessing enabling potential for highly flexible wave manipulation.

DATA AVAILABILITY

The data that support the findings of this study are available from the corresponding author upon reasonable request.

REFERENCES

[1]Y. Y. Chen and G. L. Huang, Acta Mech. Sin. **31**(3), 349 (2015).

[2]Y. Tian and Y. Shen, J. Sound Vib. **485**, 115566 (2020).

[3]Q. Zhang, K. Zhang, and G. Hu, Appl. Phys. Lett. **112**(22), 221906 (2018).

[4]R. Zhu, Y. Y. Chen, M. V. Barnhart, G. K. Hu, C. T. Sun, and G. L. Huang, Appl. Phys. Lett. **108**(1), 011905 (2016).

[5]N. Fang, D. Xi, J. Xu, M. Ambati, W. Srituravanich, C. Sun, and X. Zhang, Nat. Mater. **5**(6), 452 (2006).

[6]Z. Hou and B. M. Assouar, Appl. Phys. Lett. **106**(25), 251901 (2015).

[7]X. N. Liu, G. K. Hu, G. L. Huang, and C. T. Sun, Appl. Phys. Lett. **98**(25), 251907 (2011).

[8]R. Zhu, X. N. Liu, G. K. Hu, C. T. Sun, and G. L. Huang, Nat. Commun. **5**, 5510 (2014).

[9]Y. Chen, J. Hu, and G. Huang, J. Intell. Mater. Syst. Struct. **27**(10), 1337 (2016).

[10]Y. Chen, X. Li, H. Nassar, G. Hu, and G. Huang, Smart. Mater. Struct. **27**(11), 115011 (2018).

[11]V. Candido de Sousa, C. Sugino, C. De Marqui, Jr., and A. Erturk, J. Appl. Phys. **124**(6), 064505 (2018).

[12]T. Chen, M. Ruzzene, and A. Baz, J. Vib, Control **6**, 1065 (2000).

[13]K.-C. Chuang, X.-F. Lv, and D.-F. Wang, Appl. Phys. Lett. **114**(5), 051903 (2019).

[14]K.-C. Chuang, X.-F. Lv, and Y.-H. Wang, J. Appl. Phys. **125**(5), 055101 (2019).

[15]V. C. de Sousa, D. Tan, C. De Marqui, and A. Erturk, Appl. Phys. Lett. **113**(14), 143502 (2018).

[16]C. Liang and C. A. Rogers, J. Intell. Mater. Syst. Struct. **8**, 314 (1997).

[17]X.-F. Lv, S.-F. Xu, Z.-L. Huang, and K.-C. Chuang, Phys. Lett. A **384**(2), 126056 (2020).

[18]E. Rustighi, M. J. Brennan, and B. R. Mace, Smart. Mater. Struct. **14**(1), 19 (2005).

[19]M. Ruzzene and A. Baz, J. Vib. Acoust. **6**(7), 1065 (2000).

[20]K. Williams, G. Chiu, and R. Bernhard, J. Sound Vib. **249**(5), 835 (2002).

[21]Y. Tian, Y. Shen, D. Rao, and W. Xu, Smart. Mater. Struct. **28**(7), 075038 (2019).

[22]X. Yan, R. Zhu, G. Huang, and F.-G. Yuan, Appl. Phys. Lett. **103**(12), 121901 (2013).

[23]S.-M. Yuan, A. L. Chen, and Y.-S. Wang, J. Sound Vib. **470**, 115168 (2020).

[24]Y. Shen and V. Giurgiutiu, Wave Motion **58**, 22 (2015).

[25]V. Giurgiutiu, in *Structural Health Monitoring with Piezoelectric Wafer Active Sensors* (Elsevier, Oxford, 2014), p. 573.